HHS Public Access

Author manuscript

Nat Cell Biol. Author manuscript; available in PMC 2015 March 26.

Published in final edited form as:

Nat Cell Biol. 2015 January ; 17(1): 81–94. doi:10.1038/ncb3082.

The Rho-GTPase Rnd1 Suppresses Mammary Tumorigenesis and EMT by Restraining Ras-MAPK signaling

Tomoyo Okada[1,14,15], **Surajit Sinha**[1,14], **Ilaria Esposito**[1,14], **Gaia Schiavon**[1,16], **Miguel A. López-Lago**[1,17], **Wenjing Su**[1], **Christine A. Pratilas**[2,4,18], **Cristina Abele**[11], **Jonathan M. Hernandez**[1,5], **Masahiro Ohara**[13], **Morihito Okada**[13], **Agnes Viale**[8], **Adriana Heguy**[9,19], **Nicholas D. Socci**[10], **Anna Sapino**[12], **Venkatraman E. Seshan**[6], **Stephen Long**[3], **Giorgio Inghirami**[11,20], **Neal Rosen**[2,7], and **Filippo G. Giancotti**[1,*]

[1]Cell Biology, Sloan-Kettering Institute for Cancer Research, Memorial Sloan-Kettering Cancer Center, New York, NY 10065, USA

[2]Molecular Pharmacology and Chemistry, Sloan-Kettering Institute for Cancer Research, Memorial Sloan-Kettering Cancer Center, New York, NY 10065, USA

[3]Structural Biology Programs, Sloan-Kettering Institute for Cancer Research, Memorial Sloan-Kettering Cancer Center, New York, NY 10065, USA

[4]Department of Pediatrics, Memorial Hospital, Memorial Sloan-Kettering Cancer Center, New York, NY 10065, USA

[5]Department of Surgery, Memorial Hospital, Memorial Sloan-Kettering Cancer Center, New York, NY 10065, USA

[6]Department of Epidemiology and Biostatistics, Memorial Hospital, Memorial Sloan-Kettering Cancer Center, New York, NY 10065, USA

[7]Department of Medicine, Memorial Hospital, Memorial Sloan-Kettering Cancer Center, New York, NY 10065, USA

[8]Genomics, Memorial Sloan-Kettering Cancer Center, New York, NY 10065, USA

[9]G. Beene Translational Oncology, Memorial Sloan-Kettering Cancer Center, New York, NY 10065, USA

[*]Correspondence: f-giancotti@ski.mskcc.org.
[14]These authors contributed equally
[15]Present address: Department of Surgery, MSKCC.
[16]Present address: Breast Unit, Royal Marsden Hospital, London, UK SW3 6JJ.
[17]Present address: Department of Surgery and Center for Cell Engineering, MSKCC.
[18]Present address: The Sidney Kimmel Comprehensive Cancer Center, Johns Hopkins University School of Medicine, Baltimore, MD
[19]Present address: Department of Pathology, Office for Collaborative Science, New York University, NY.
[20]Present address: Department of Pathology and Laboratory Medicine, Weill Cornell Medical College, New York

AUTHOR CONTRIBUTIONS

T. Okada, S. Sinha, I. Esposito, G. Schiavon, M. Lopez-Lago, W. Su, C. A. Pratilas, J. Hernandez, and C. Abele performed and interpreted experiments; M. Ohara, M. Okada, and A. Sapino provided annotated breast tumor samples, A. Viale designed and performed genomic analyses; G. Schiavon and V. Seshan performed bioinformatic analyses; S. Long provided structural insight; G. Inghirami examined the results of FISH experiments; N. Rosen and G. Inghirami supervised some of the experiments; F.G. Giancotti supervised the entire study and wrote the paper.

[10]Bioinformatics Core Facilities, Memorial Sloan-Kettering Cancer Center, New York, NY 10065, USA

[11]Department of Biomedical Sciences and Human Oncology, Center of Experimental Medicine and Research, University of Torino, Torino 10126, Italy

[12]Department of Medical Sciences, Center of Experimental Medicine and Research, University of Torino, Torino 10126, Italy

[13]Department of Surgical Oncology, Research Institute for Radiation Biology and Medicine, Graduate School of Biomedical Sciences, Hiroshima University, Hiroshima, Japan

SUMMARY

We identified the Rho-GTPase Rnd1 as a candidate metastasis suppressor through bioinformatics analysis and showed that its depletion disrupt epithelial adhesion and polarity, induced Epithelial-to-Mesenchymal Transition (EMT), and cooperated with deregulated expression of c-Myc or loss of p53 to cause neoplastic conversion. Mechanistic studies revealed that Rnd1 suppresses Ras signalling by activating the GAP domain of Plexin B1, which inhibits Rap1. Rap1 inhibition in turn led to derepression of p120-RasGAP, which was able to inhibit Ras. Inactivation of Rnd1 in mammary epithelial cells induced highly undifferentiated and invasive tumors in mice. Conversely, Rnd1 expression inhibited spontaneous and experimental lung colonization in mouse models of metastasis. Genomic studies indicated that gene deletion in combination with epigenetic silencing or, more rarely, point mutation inactivates *RND1* in human breast cancer. These results reveal a previously unappreciated mechanism through which Rnd1 restrains activation of Ras-MAPK signaling and breast tumor initiation and progression.

INTRODUCTION

Oncogenes such as Ras and BRAF deregulate mitogenesis but also induce senescence, which must be evaded through the acquisition of cooperating oncogenic mutations, such as loss of p53 or Rb [1]. In the breast and other organs, progression to frank malignancy requires loss of epithelial adhesion and polarity and acquisition of an invasive phenotype [2]. In some cases, tumor cells hijack a developmental program of gene expression, the EMT, to gain an invasive capacity and disseminate [3]. The genetic or epigenetic alterations driving tumor initiation and progression in the most aggressive subtypes of breast cancer – basal-like and triple negative (TN) - are incompletely understood.

Tumor initiation and EMT appear to be driven by distinct genomic alterations. Expression of mutant Ras from a knock-in allele or constitutive activation of ErbB2 coordinately disrupt epithelial adhesion, polarity and growth control, but do not induce full EMT in mammary epithelial cells [4–6]. Additionally, inactivation of the polarity proteins Scribble and Par 3 induces partial disruption of epithelial polarity, but not overproliferation [7, 8]. In contrast, transcription factors, such as Snail and Twist, cause EMT but do not initiate transformation [4, 9, 10].

Rho-GTPases regulate epithelial adhesion and polarity, cell migration, membrane traffic, and the cell division cycle [11]. Although infrequently mutated in most cancers, Rho, Rac and

Cdc42 function downstream of mutant Ras to mediate transformation and to orchestrate the cytoskeletal changes required for tumor invasion [12]. As they govern several aspects of epithelial adhesion and polarity, Rho-GTPases could also function as tumor suppressors. Here we show that inactivation of Rnd1 simultaneously induces mammary tumor initiation and EMT by activating oncogenic Ras-MAPK signalling.

RESULTS

Rnd1 is a Potential Suppressor of Breast Cancer Progression

To identify Rho-GTPases involved in breast tumor suppression, we used bioinformatic analysis and RNAi-mediated silencing. Kaplan-Meyer analysis of the MSKCC DNA microarray dataset, comprising predominantly advanced ER^- primary breast cancers [13], revealed that low levels of *RHOD* and *RND1*, but neither low nor high levels of other Rho GTPase transcripts, predict metastasis (Fig. 1a and Supplementary Table 1). Although Rnd1 and RhoD have not been implicated in tumorigenesis, 12q12-q13, which comprises *RND1*, is frequently deleted in pancreatic and adenoid cystic carcinomas [14, 15]. Silencing of Rnd1 induced scattering of cultured human mammary epithelial MCF-10A cells, disruption of adherens junctions, internalization and downregulation of E-cadherin, upregulation of N-cadherin and fibronectin, and a partial switch from the epithelial to the mesenchymal isoform of p120-catenin [16] (Fig. 1b–f). Q-PCR confirmed that E-cadherin was repressed by a transcriptional mechanism and potentially implicated the matrix metalloproteases MMP2 and MMP3 and the transcription factors Snail1, Zeb1, Zeb2, and Foxc2 in these phenotypic and functional changes (Fig. 1g). Control experiments confirmed the specificity and generality of these effects (Supplementary Fig. 1a–j). In contrast, silencing of RhoD induced apoptosis, but no scattering, as assessed by morphological criteria, (Supplementary Fig. 1k, l). Thus, depletion of Rnd1, but not RhoD, causes an EMT.

Underexpression of Rnd1 correlated with expression of the 70-gene poor-prognosis signature [17] or the lung metastasis signature [13] in the MSKCC dataset (Supplementary Fig. 1m) and was associated with increased risk of both lung and bone metastasis, suggesting that Rnd1 inhibits tissue invasion rather than organ-specific metastasis (Supplementary Fig. 1n, o). Q-PCR analysis of cancer cell lines and Oncomine analysis of breast cancer datasets revealed that *RND1* is expressed at significantly lower levels in the most aggressive subtypes of breast cancer (ER^-, basal-like, and TN) (Figure 1h and supplementary Fig. 1p). Kaplan-Meyer analysis of a dataset comprising 2,324 patients [18] indicated that under-expression of Rnd1 correlates with a significantly reduced time to progression in ER^- but not ER^+ patients (Fig. 1i). Multivariate analysis indicated that under-expression of Rnd1 constitutes a strong, independent, negative prognostic factor (Supplementary Table 2). These observations identify Rnd1 as a potential suppressor of tumor progression and metastasis.

Inactivation of Rnd1 Causes Hyperproliferation Followed by Senescence

Rnd proteins are constitutively activated Rho-GTPases, which exert cell type-specific effects on signaling and cytoskeletal organization by interacting with multiple target-effectors [19]. Since we could not identify or generate high-affinity antibodies reacting specifically with endogenous Rnd1 (Fig. 1b; Methods), we used Q-PCR to examine if its expression varies

during the cell cycle. Mitogens caused a progressive decline of Rnd1 mRNA, whereas exposure to TGF-β, contact inhibition, and UV treatment exerted the opposite effect, suggesting that Rnd1 inhibits cell cycle progression (Supplementary Fig. 2a). Consistently, depletion of Rnd1 elevated the levels of phospho-Rb, Cyclin A, and phospho-Histone H3 and the expression of cell cycle genes and increased cell cycle progression at day 3 post-infection, while ectopic expression counteracted these effects (Fig. 2a, b and Supplementary Fig. 2b-e and Supplementary Table 3). At later time points, the percentage of Rnd1-silenced cells in S phase declined below control values, whereas the percentage of those in G2/M remained elevated (Fig. 2b). Following replating, the Rnd1-silenced cells underwent complete growth arrest and senescence (Fig. 2c–f). Thus, inactivation of Rnd1 provokes transient hyperproliferation followed by premature senescence, as seen in strong oncogenic lesions.

Oncogene-induced senescence arises from aberrant DNA replication as well as production of reactive oxygen species (ROS), which cause DNA damage [20]. Rnd1-silenced MCF-10A cells exhibited activated CHK2, phosphorylated H2A.X, and elevated expression of genes involved in the DNA damage response, Ras-induced mitotic stress, and EMT [21] (Fig. 2g, Supplementary Fig. 2d, f; and Supplementary Table 3). These cells accumulated elevated levels of ROS and treatment with glutathione (GSH) rescued them from senescence, suggesting that ROS-mediated DNA damage contributes to their senescence (Fig. 2h, i). MCF-10A cells do not express p16 and p15 because of homozygous deletions at the *CDKN2A* and *CDKN2B* loci[22]. Rnd1 silencing led to accumulation of p27, but not p53 or p21 in these cells, and silencing of p27 rescued them from senescence, causally linking p27 to the induction of senescence in this setting (Supplementary Fig. 2g and Fig. 2j).

Myc Rescues the Rnd1-silenced Cells from Senescence and Enables their Neoplastic Conversion and Invasive Outgrowth

Prolonged culture enabled us to isolate clones of Rnd1-silenced MCF-10A cells, which had escaped senescence and were able to grow in soft agar (Supplementary Fig. 3a, b). These cells exhibited elevated c-Myc but not p27, suggesting that Myc may rescue the Rnd1-silenced cells from senescence by suppressing p27 [23] (Supplementary Fig. 3c). Indeed, ectopic expression of Myc downregulated p27 and enabled the MCF-10A cells to escape from senescence and undergo transformation following inactivation of Rnd1 (Fig. 3a–d and Supplementary Fig. 3d–f). HMLE cells did not undergo senescence following Rnd1 depletion, presumably because they overexpress telomerase and lack Rb and p53 function [24], but instead exhibited robust soft agar growth (Supplementary Fig. 3g, h), confirming that loss of Rnd1 induces neoplastic transformation.

Expression of Myc enabled MCF-10A cells to form filled pseudo-acini with a significant degree of epithelial organization in 3D Matrigel, as anticipated [8] (Fig. 3e, f). Additional inactivation of Rnd1 produced disorganized, expansive multi-acinar structures surrounded by a halo of dispersed cells (Fig. 3e, f). These structures had partially disorganized adherens junctions (E-cad) and a discontinuous or absent basement membrane (Lam-5). Isolated cells and groups of cells had detached from the multi-acinar structures consistent with basement membrane defects and invaded through Matrigel (Lam-5, arrow). These cells and those still

within the structures had re-oriented their Golgi apparatus toward the Matrigel (GM130, small arrows). Whereas the pseudo-acinar structures induced by Myc underwent limited expansion because Myc induces modest overproliferation balanced by apoptosis [5, 8], the multi-acinar stuctures formed by Rnd1-silenced cells underwent significant expansion as a result of significant overproliferation (Supplementary Fig. 3i–l). Thus, inactivation of Rnd1 promotes hyperproliferation, disruption of epithelial adhesion and polarity, and invasion.

Depletion of Rnd1 Activates Ras Signaling

Rnd proteins indirectly inhibit the activation of Rho and Ras GTPases, in a cell context-dependent manner [19]. Rnd1 silencing, however, did not activate Rho proteins in MCF-10A cells (Supplementary Fig. 4a). Considering the similarity of the effects induced by inactivation of Rnd1 and activation of Ras [25], we examined the possibility that Rnd1 suppresses Ras signaling. GST-RBD pull down indicated that Ras is robustly activated in MCF-10A cells at 2 and 5 days after Rnd1 shRNA depletion (Fig. 4a) and blotting with isoform-specific antibodies demonstrated activation of both H-Ras and K-Ras (Fig. 4b). Ras activation was particularly evident in the absence of mitogens and following peak stimulation with mitogens. This was also observed in HMLE cells, human umbilical vein endothelial cells (HUVECs), and HEK 293-T cells, attesting to its generality (Supplementary Fig. 4b, c).

In spite of its ability to activate Ras, depletion of Rnd1 did not rapidly activate the Raf-ERK cascade or AKT. Instead, short-term depletion of Rnd1 suppressed MEK and ERK activation in MCF-10A cells (Fig. 4a; compare days 2 and 5). Acute depletion of the Ras-GAP NF1 induces a similar effect because excessive Ras signaling is antagonized by strong negative feedback loops, which contribute to the induction of senescence [26]. In agreement with this interpretation, Rnd1 silencing upregulated several Ras target genes, which encode negative regulators of the Ras-ERK pathway, such as Sprouty, Spred, and MAPK phosphatases (Fig. 4c). Furthermore, MEK and ERK inhibition correlated with CHK2 activation Rnd1-silenced cells (Fig. 4a). Cells escaping from senescence after NF1 depletion are no longer restrained by negative feedback loops acting on Ras signaling and display hypersensitivity to mitogenic stimulation [26, 27]. Similarly, Rnd1 depletion sustained the activation of the Raf-ERK pathway and AKT in response to EGF in Rnd1-silenced MCF-10A cells that had bypassed senescence (Fig. 4d). Thus, inactivation of Rnd1 induces robust activation of Ras and, following disengagement of negative feedback loops, enhances sensitivity of the Raf-ERK cascade to mitogenic stimulation.

Loss of Rnd1 Promotes Neoplastic Transformation and EMT through Raf-ERK Signaling

To examine if loss of Rnd1 promotes neoplastic transformation and EMT by activating Ras signaling, we used pharmacological inhibition. Inhibition of MEK with PD98059 or UO126 blocked the disassembly of adherens junctions in Rnd1-silenced cells, but inhibition of PI-3K with Wortmannin or Rac with NSC23766 did not (Fig. 4e and Supplementary Fig. 4d). Inhibition of the Rho effectors Rho-Kinase and Myosin II with Y27632 and Blebbistatin, respectively, caused partial disassembly of adherens junctions in control cells, as anticipated from the requirement for Rho signaling in their assembly [28], and did not interfere with their disruption following Rnd1 depletion (Supplementary Fig. 4e).

Furthermore, inhibition of MEK suppressed the ability of Rnd1-silenced cells expressing Myc to undergo accelerated cell cycle progression, to grow in soft agar, and to invade through Matrigel, whereas inhibition of PI-3K inhibited these processes to a lesser extent (Fig. 4f, g and Supplementary Fig. 4f). These results indicate that Rnd1 inactivation promotes neoplastic transformation and EMT by activating Raf-ERK signaling, consistent with the involvement of this pathway in both processes [29].

To examine the clinical relevance of our observations, we analysed the EMC192, EMC286, and MSKCC99 breast cancer DNA microarray datasets [13]. Gene Set Enrichment Analysis (GSEA) indicated that under-expression of *RND1* correlated with expression of a Ras signature in all three datasets and with expression of a Myc signature in two of them, but not with expression of a Src or a β-catenin signature in any dataset (Fig 4h and Supplementary Fig. 4g). Underexpression of *RND1* correlated with overexpression of *MYC* in all the datasets, corroborating the hypothesis that loss of Rnd1 cooperates with deregulation of c-Myc in human breast cancer (Supplementary Fig. 4h). These findings suggest that inactivation of Rnd1 underlies aberrant activation of Ras signaling and cooperates with deregulated Myc in human breast cancer.

Rnd1 Inhibits Ras Signaling by Activating the GAP Domain of Plexin B1

Rnd proteins bind to p190-RhoGAP and activate its GAP activity toward RhoA, causing disassembly of stress fibers and focal adhesions in fibroblasts [30]. In addition, Rnd1, but not Rnd2 or 3, combines with and activates the cytoplasmic GAP domain of Plexin B1 to mediate growth cone collapse in neurons treated with Sema4D [31]. To examine the mechanism by which Rnd1 suppresses proliferation, we mutated four evolutionarily conserved residues in its effector loop and identified two loss-of-function mutations, T45A and E48A (Fig. 5a, b). These mutations disrupted the association of Rnd1 with Plexin B1 but not p190-RhoGAP. In contrast, the other two mutations did not affect binding to Plexin B1 or p190-RhoGAP (Fig. 5c). These results suggest that Rnd1 suppresses cell proliferation by activating the GAP domain of Plexin B1.

Plexin B1 is expressed at similar levels in both normal and neoplastic breast epithelial cells, whereas the levels of its ligand Sema4D are upregulated in breast cancer cells (Supplementary Fig. 5a), consistent with the hypothesis that Sema4D promotes tumor angiogenesis by engaging Plexin B2 on endothelial cells [32]. Plexin B1 silencing caused robust activation of Ras and phenotypic and functional changes associated with the EMT in MCF-10A cells (Fig. 5d–f and Supplementary Fig. 5b), consistent with the hypothesis that Rnd1 suppresses Ras by activating Plexin B1. Although Plexin B1 has been reported to combine with ErbB2 and c-Met to influence their signaling capacity [33, 34], treatment with Sema4D did not modify c-Met signaling in HMLE cells or HER2 signaling in ZR751 cells (Supplementary Fig. 5c, d). These results suggest that Rnd1 suppresses Ras signaling and the EMT by activating the GAP domain of Plexin B1.

Plexin B1 Inhibits Rap1 and Activates p120 Ras GAP

As Plexin B1 exerts a potent GTPase activity toward Rap1, but not R-Ras, M-Ras, or H-Ras [35, 36], we hypothesized that the Rnd1-Plexin B1 complex suppresses Ras by inhibiting

Rap1. In agreement with a requirement for Rnd1 in Plexin B1 function, siRNA-mediated depletion of Rnd1 caused activation of Rap1 in MCF-10A cells (Fig. 6a, b). Moreover, wild-type Rap1 and, even more so, constitutively active Rap1-V12 induced GTP loading on Ras and ensuing activation of CRAF, MEK, and ERK (Fig. 6c). Finally, simultaneous inactivation of all Rap1 and Rap2 isoforms via expression of Rap1-GAP attenuated the basal activation of Ras in control MCF-10A cells and reversed the over-activation of Ras induced by depletion of Rnd1 (Fig. 6d). These results suggest that depletion of Rnd1 activates Ras by increasing GTP-loading on Rap1.

Intriguingly, GTP-Rap1 binds tightly to p120-RasGAP (encoded by *RASA1*) without undergoing GTP hydrolysis, making Rap1 an effective inhibitor of p120-RasGAP [37, 38]. Thus, the Rnd1-Plexin B1 complex may inhibit multiple Ras isoforms by inhibiting Rap1 and thereby activating p120-RasGAP. In agreement with this hypothesis, TCGA datasets indicated that *RND1*, *PLXNB1*, and *RASA1* are under-expressed in largely non-overlapping and sizeable subsets of basal-like, but not luminal, breast cancers (Supplementary Fig. 6a). Furthermore, Rap1-V12 associated with p120-RasGAP, whereas wild type Rap1 and Rap1-N17 did not (Fig. 6e). Finally, p120-RasGAP depletion caused robust activation of Ras, but not CRAF, MEK or ERK, in MCF-10A cells, consistent with an engagement of negative feedback loops (Fig. 6f and Supplementary Fig. 6b). Collectively, these results suggest that the Rnd1-Plexin B1 complex inhibits Rap1 and, hence, de-represses p120 Ras-GAP, leading to inhibition of Ras (Fig. 6g).

Inactivation of Rnd1 Induces Mammary Tumor Initiation and Progression In Vivo

To study the tumor suppressor function of Rnd1 in vivo, we silenced its expression in mouse Comma-D cells, which possess a subpopulation of ductal-alveolar progenitor cells and can regenerate seemingly normal mammary glands upon injection in the mammary fat pad [39]. Upon silencing of Rnd1, these cells underwent phenotypic and functional changes consistent with EMT and acquired the ability to grow in soft agar but did not become senescent, presumably because they are *Tp53* mutant [40] or overexpress c-Myc (Supplementary Fig. 7a–g). Intriguingly, whereas control cells formed seemingly normal glandular structures following orthotopic injection in vivo, the Rnd1-silenced cells produced highly undifferentiated and locally invasive tumors characterized by defective deposition of laminin, loss of expression of E-cadherin, and increased expression of vimentin (Fig. 7a, b). In spite of their invasive ability, the Rnd1-silenced Comma-D cells did not colonize the lung within 6 weeks after tail-vein injection, consistent with the hypothesis that the EMT opposes metastatic reactivation [41]. We thus asked if expression of Rnd1 could inhibit tumor cell dissemination and metastatic colonization. Bioluminescent imaging indicated that ectopic expression of Rnd1 suppresses the ability of ErbB2-transformed and 4T1 mammary tumor cells to colonize the lung following tail-vein injection (Fig. 7c and Supplementary Fig. 7h–j; >99% inhibition). To examine the ability of Rnd1 to inhibit spontaneous metastasis, we injected control and Rnd1-expressing 4T1 cells orthotopically. Having found that Rnd1 delays primary tumor growth (Fig. 7d), we surgically removed bilateral tumors that had grown to a similar cumulative size in both cohorts and evaluated lung colonization after 1 week (Fig. 7e). The results indicated that Rnd1 suppresses spontaneous metastasis to the

lung (Fig. 7f and Supplementary Fig. 7k). These experiments indicate that Rnd1 suppresses tumor initiation and progression in vivo.

Deletion and Epigenetic Inactivation of *RND1* in Human Breast Cancer

FISH revealed allelic losses at the *RND1* locus in 17% of primary breast carcinomas from the University of Torino (Fig. 8a and Supplementary Fig. 8a). In addition to hemizygous losses, we detected reduced copy numbers in the context of Chr. 12 polysomy, suggesting that selective pressures drive deletion of *RND1* even within an amplicon [42]. The percentage of tumor cells with hemizygous deletions at the *RND1* locus was in many instances large (up to 73%) and in 55% of the cases >20% of the remaining tumor cells displayed Chr. 12 monosomy (Supplementary Fig. 8a and Table S4). However, we did not identify homozygous deletions, suggesting that additional mechanisms contribute to inactivate *RND1* in breast cancer.

To examine the contribution of epigenetic mechanisms, we treated a subset of luminal and basal-like cell lines expressing very low levels of Rnd1 with the DNA methylation inhibitor 5-aza-2-deoxycytidine (5-Aza), the Histone De-ACetylase (HDAC) inhibitor SAHA, or both compounds. Simultaneous exposure to both inhibitors led to a large increase in expression of *RND1* in the basal-like lines, indicating that both promoter methylation and histone deacetylation suppress expression of *RND1* in these lines (Supplementary Fig. 8b). In contrast, the inhibitors were largely ineffective, even when combined, in most luminal lines (Supplementary Fig. 8b). SAHA alone rescued the expression of *RND1* in the HCC1428 cells, which are ER^+ but carry mutant *BRCA2*, a lesion typically occurring in triple-negative cancers [43]. Epityper analysis confirmed that the promoter of *RND1* is methylated extensively in HCC1569 cells and to a more limited degree in MBA-MB468 and BT474 cells (Supplementary Fig. 8e). 3-Deazaneplanocin A (DZNep) [44], which induces specific degradation of Polycomb Repressor Complex 2 components, cooperated with SAHA to rescue expression of *RND1* in the MDA-MB468, HCC1428, and BT474 cells (Fig. 8b). Other cell lines underwent rapid apoptosis with DZNep [44]. Silencing of the PRC2 component EZH2 produced similar effects (Supplementary Fig. 8f, g). Finally, EZH2 bound to the *RND1* promoter and deposited its repressive mark, H3K27me3, in HCC1569 and HCC1428 cells, but not ZR751 and MCF-10A cells (Fig. 8c). These results suggest that promoter methylation and PRC2-mediated silencing contribute to suppressed expression of *RND1* in breast cancer cells.

Mutations of *RND1* in Human Breast Cancer

To examine if missense or nonsense mutations contribute to clonal inactivation of *RND1* in breast cancer, we subjected 96 breast cancers from the University of Hiroshima to targeted deep sequencing by SOLiD and identified 4 missense mutations, which replaced evolutionarily conserved amino acids of Rnd1 (Fig. 8d and Supplementary Table 5). Structural considerations suggest that the *G70R* mutation, which replaces a switch II residue that is highly conserved among Ras-like GTPases, disrupts GTP binding and possibly interaction with the GAP domain of Plexin B1 [45] (Fig. 8d, e). Furthermore, the *F180C* mutation, which also maps to a highly conserved residue, may impair the folding of Rnd1, reducing guanine nucleotide binding (Fig. 8d, e). BrdU incorporation experiments indicated

that G70R, E98D, and F180C do not possess growth inhibitory activity, whereas M185V retains partial growth inhibitory activity (Fig. 8f).

Epitope tagging experiments indicated that Rnd1 colocalizes with H-Ras in the Golgi and at the plasma membrane and with K-Ras within a vesicular compartment surrounding the Golgi and at the plasma membrane, suggesting that Rnd1 follows a biosynthetic and export route similar to that of Ras proteins [46] (Supplementary Fig. 8c, d). Although M185V localized in the Golgi and at the plasma membrane like wild type Rnd1, G70R and F180C accumulated in large cytosolic aggregates and E98D displayed an intermediate phenotype (Fig. 8g). Cycloheximide chase experiments indicated that the half-life of the mutants was decreased in a manner proportional to their functional inability to accumulate at the membrane (Fig. 8h). Transfection of 5-fold excess expression vector resulted in clearly detectable steady state levels of G70R, E98D, and F180C but did not induce their association with Plexin B1 (Fig. 8i). In contrast, M185V combined with Plexin B1. These results suggest that G70R, E98D, and F180C have lost growth suppressive activity as a result of defective folding, export to the plasma membrane, and association with Plexin B1. Together, these findings indicate that hemizygous deletion in combination with silencing or, more rarely, mutation contributes to the inactivation of the tumor suppressor function of *RND1* in breast cancer.

DISCUSSION

We found that Rnd1 loss robustly activates Ras and provokes unscheduled proliferation and EMT in the mammary epithelium, and linked these events to activation of the Raf-ERK cascade. Similar to mammary epithelial cells overexpressing mutant Ras [47, 48], those depleted of Rnd1 underwent senescence unless they were induced to overexpress c-Myc or had lost p53 function. In the presence of these cooperating oncogenic alterations, inactivation of Rnd1 simultaneously induced neoplastic conversion and EMT. These findings indicate that Rnd1's inhibition of Ras prevents unscheduled proliferation and disruption of epithelial adhesion and polarity in mammary epithelium.

Our mechanistic studies provided evidence that Rnd1 suppresses oncogenic Ras signaling by activating the GAP domain of Plexin B1, which inhibits Rap1 [36]. As GTP-loaded Rap1 binds to p120-RasGAP [35], blocking its ability to inhibit multiple Ras proteins [37, 38], we examined if the Rnd1-Plexin B1 complex inhibits Ras by inactivating Rap1 and hence activating p120-RasGAP. Inactivation of Rap1 suppressed the activation of Ras induced by silencing of Rnd1. In addition, activated Rap1 combined with p120-RasGAP and activated Ras and silencing of p120 Ras-GAP caused robust activation of Ras. Thus, inactivation of Rnd1 and, hence, of Plexin B1 GAP domain activates Rap1, which in turn blocks p120 Ras-GAP, leading to activation of Ras. However, since Rap1 has an effector domain identical to that of Ras and activates shared target-effectors, including BRAF but not CRAF, it can buttress activation of ERK in mammalian cells expressing BRAF[49–51] or in drosophila, which express a single isoform of RAF similar to mammalian BRAF[52]. It is therefore possible that inactivation of Rnd1 sustains signaling to ERK also through Rap1-mediated activation of BRAF. In agreement with the hypothesis that Rap1 signals to ERK in mammary epithelial cells, overexpression of Rap1 activated ERK and induced disruption of

epithelial adhesion and polarity and invasion in mammary epithelial HMT-3522 cells placed in 3D Matrigel [53]. Although inhibition of Ras provides a compelling explanation for the tumor suppressor function of Rnd1, we cannot formally exclude the possibility that Rnd1 opposes neoplastic conversion and EMT also by additional mechanisms.

Although *RAS* mutations are relatively infrequent in breast cancer [54], approximately 50% of breast tumors exhibit a constitutively activated Ras-ERK pathway [55]. Our results indicate that genetic and epigenetic inactivation of *RND1* underlies activation of the Ras-ERK pathway in a subset of these cancers. Notably, prior studies have indicated that Plexin B1 functions as a tumor suppressor in melanoma cells [56, 57] and genomic sequencing has identified missense mutations in *PLXNB1* and other Plexin genes in breast and prostate cancer [58, 59]. Two prevalent mutations disrupt the interaction of Plexin B1 with Rnd1 [60]. Finally, TCGA analysis indicates that *RND1* suffers from potentially inactivating point mutations in melanoma (3.9%), and *PLXNB1* in melanoma (8.3%), colorectal cancer (11.1%), and lung adenocarcinoma (4.4%) [61], suggesting that the tumor suppressor pathway we have identified may be inactivated in several tumor types driven by aberrant Ras signaling. We propose that MEK inhibitors or other agents targeting the Ras-ERK signaling axis could potentially display efficacy in cancers carrying inactivating alterations in *RND1* or *PLXB1*.

METHODS

Cells and Transfection

HMLE cells were obtained from Robert Weinberg (Whitehead Institute, MIT, Cambridge, MA) and MCF-10A cells from Joan Brugge (Harvard University, Boston, MA). The COMMA-Dβ-geo cells from Daniel Medina (Baylor College of Medicine, Houston, TX) were cultured in DMEM supplemented with 2% Fetal Calf Serum, Insulin (10 μg/ml), EGF (5 ng/ml) and PSFG. HMLE and MCF10-A cells were cultured in MEGM (Lonza). 4T1 cells from Fred R. Miller (Wayne State University, Detroit, MI) were cultured in DMEHG supplemented with 10% FBS. Human breast cancer cell lines were cultured as described previously [62]. The mouse ErbB2-transformed mammary tumor cells were derived from an MMTV-*Neu(YD)* mouse and reconstituted with a wild type form of the rat Neu oncogene under the control of the CMV promoter [6]. Lipofectamine 2000 (Invitrogen) and electroporation (Amaxa) were used to transfect HEK 293T cells and HUVECs, respectively.

Antibodies and Reagents

Since previously described antibodies did not possess sufficient affinity and specificity to allow detection of endogenous Rnd1, but not Rnd2 or 3, we generated antibodies to Rnd1 by immunizing 2 rabbits with a GST-fusion protein comprising full-length Rnd1. The rabbit antiserum that displayed the highest affinity to recombinant Rnd1 and no crossreaction with Rnd2 or Rnd3 was adsorbed on GST-Sepharose and then affinity purified on Sepharose-conjugated GST-Rnd1. These affinity-purified antibodies reacted selectively with recombinant Rnd1, but not Rnd2 or Rnd3, but did not detect endogenous Rnd1 in multiple cell lines. All other antibodies used are listed in Supplementary Table 6. ROS were detected using the fluorescent indicator carboxy-H_2DCFDA (dichlorodihydrofluorescein diacetate,

BD Molecular Probe). The MEK inhibitor U0126 was from Promega and PD98059 from Calbiochem. The PI-3K inhibitor LY294002 was from Cell Signaling and Wortmannin from Sigma. The Rac inhibitor NSC23766 was from Calbiochem. The ROCK inhibitor Y-27632 dehydrochloride from AXXORA. Glutathione Monoethyl Ester was from SIGMA. SA-β-galactosidase activity was detected using the Senescence β-Galactosidase Staining Kit from Cell Signaling. HGF was from GIBCO, Sema4D from Sino Biological, HRG from R&D. The demethylating agent 5-aza-2-deoxycytidine (5-Aza) was from Calbiochem, the HDAC inhibitor SAHA from Sigma, and DZNep from Cayman. Cells were plated onto tissue culture plates for 48 hours and then treated with 5 or 10 μM 5-Aza for 72 hours followed by SAHA for 24 hours (5 μM), or with each agent alone, and harvested for Q-PCR. HCC1428, MDA-MB468, and BT474 cells were treated with DZNep for 48 hrs (5 μM) followed by 5-Aza-2′ deoxycytidine for 72 hours (10 μM) and HDAC inhibitor SAHA for 24 hours (5 μM), or with various combinations thereof.

Viral Transduction

For silencing, viral supernatants were generated by transfecting 293-FT cells with the shRNA constructs in combination with the packaging vectors pVSVG and pDR2. pLKO.1 plasmids encoding short hairpin RNAs targeting human Rnd1 (clones TRCN0000018338 and TRCN0000039977) and targeting PlexinB1 (clones TRCN0000061533 and TRCN0000061537) were from Open Biosystems; shRNAs targeting mouse Rnd1 (clones TRCN0000089694 and TRCN0000089695) and p27 (clone TRCN0000039928 and TRCN0000039930) were from Sigma and those targeting RhoD (SKI-RSI-197446, SKI-RSI-246157) from the HTSC of MSKCC. si-RNAs targeting Rnd1 (J-008929-05), p120-RasGAP (M-005276-01) and non-targetting control (D-001810-10-05) were from Dharmacon. For ectopic exprerssion, Rnd1 was subcloned from pRK5-Rnd1 from Ann Ridley (King's College London, UK) into pBABE (Neomycin selection), pBABE-HA (puromycin selection) and pQCIX (Neomycin selection). pVSVG-PlexinB1 and pKH3-HA-P190-RhoGAP were from Luca Tamagnone (University of Turin, Italy) and Marilyn Resh (MSKCC, NY), respectively. The lentiviral vector pLV-DsRED-Myc was from Robert Weinberg. pEGFP-H-Ras and pEF-BOS-Flag-K-Ras, pEF-BOS-HA-Rap1WT and Rap1-V12 were from Tohru Kataoka (Kobe University, Japan). pcDNA3-HA-Rap1-N17 was from Xuewu Zhang (Southwestern University, Dallas, TX). pLOC-Rap1-GAP was from Open Biosystems and pLV-Flag-P120RasGAP from Genecopoeia. Mutagenesis was performed with Quick Change (Qiagen).

3D Matrigel and Soft Agar Assays

Cells were cultured in growth factor-reduced reconstituted basement membrane (Matrigel; BD Biosciences) as described previously [63]. Acini were fixed in 4% PFA and subjected to immunostaining. Images were taken with a Leica inverted confocal microscope (Leica TCS AOBS SP2). Each assay consisted of four replicate wells. Sections from 4 to 5 organoids per well were examined to determine the percentage of cleaved-caspase 3 and Ki-67 positive cells. For invasion assays, 1×10^5 cells were placed in serum-free MEGM on Transwell inserts coated with 2 mg/ml Matrigel. After incubation for 24 hours, the inserts were cleaned to remove non-invasive cells, fixed with 4% PFA, and stained with crystal violet. The absorbance of the eluted dye was measured at A_{595}. Each assay consisted of two or three

replicate wells and was repeated at least twice. For soft agar assays, 2×10^4 or 1×10^5 MCF-10A, HMLE cells, and CommaD cells were suspended in 0.35% agar in 6-well Ultra Low Cluster Plates (Costar). Each assay consisted of two or three replicates and was repeated at least twice.

Tumorigenicity and Metastasis Assays

Orthotopic injections in the mammary fat pad and experimental metastasis assays were performed as previously described [6]. Briefly, 1×10^6 CommaD cells suspended in 50 μl of PBS and Matrigel (1:1) were injected in to the mammary fat pad of 6–8 weeks female NOD/SCID mice. Tumor volumes were measured by caliper at indicated time points. To measure spontaneous metastasis, 4T1 cells transduced with TGL vector were re-suspended at 1×10^4 in 50 μl PBS and injected into the mammary gland no. 4 of BALB/c mice. Primary tumor growth was monitored weekly by taking measurements of tumor length (L) and width (W). Tumor volume was calculated using the formula Volume = $(\text{width})^2 \times \text{length}/2$. For lung colonization experiments, cells transduced with TGL vector were trypsinized, washed with PBS twice, re-suspended at 5×10^5 (ErbB2 cells) or 1×10^5 (4T1 cells) in 50 μl of PBS, and injected in the tail vein of 5–6 week-old female nude mice. Bioluminescent imaging and HE staining were used to measure lung colonization. For bioluminescent imaging, mice were anaesthetized and injected retro-orbitally with 1.5 mg of D-luciferin at the indicated times after xenografting. Animals were imaged in an IVIS 100 chamber withing 5 min after D-luciferin injection and data were recorded using Living Image software (Xenogen). To measure lung colonization, photon flux was calculated for each mouse by using a circular region of interest encompassing the thorax of the mouse after subtracting the background. ImageJ software was used to calculate the percentage area of whole lung with metastatic lesions.

Biochemical assays

Immunoprecipitation and immunoblotting experiments were conducted as described previously [6]. To analyze Ras pathway activity, MCF10A cells were starved in MEBM with 0.2 % FBS for 24 hours, then stimulated with 5 ng/ml of EGF for the indicated times. Cells were lysed in SDS-buffer, protein concentration was measured, and equal amounts of protein were loaded on SDS-PAGE and subjected to immunoblotting. To measure the active forms of Ras and RhoGTPases, the GTP bound-forms of each small GTPase were pulled down from 200 μg of total proteins by using 30 μg of GST-Raf-RBD for Ras and GST-RalGDS-RID for Rap1. 800 μg of total proteins were used to pull down active Rac and Cdc42 with GST-Pak67-150 and active Rho with GST-RBD of Rhotekin. Bound fractions were subjected to immunoblotting with antibodies against relevant Ras and Rho GTPases.

Immunostaining

Paraffin-embedded sections were subjected to immunohistochemistry and immunofluorescent staining using the automated Leica staining system at the MSKCC Molecular Cytology Core Facility.

QPCR and DNA Microarray Analysis

Total RNA was extracted using the RNeasy Mini Kit (QIAGEN) and reverse transcribed using SuperScript III, First Strand Synthesis Super Mix (Invitrogen). Q-PCR was performed with the Taqman Universal PCR Master Mix and probes from the Taqman Gene Expression Assay system (Applied Biosystems) in triplicate. See Supplementary Table 7 for taqman probes. The MSKCC dataset and the complete clinical data file were downloaded from the Gene Expression Omnibus (GEO) website (http://www.ncbi.nlm.nih.gov/geo/) by using accession number GSE2603. Affymetrix CEL files were imported in Partek Genomic Suite 6.4 software (Partek Inc.) by using the Robust Multichip Average (RMA) method. Log2 transformed data of the probesets for RhoGTPases (Rnd1 included) and Myc (202431_s_at) were used for the analysis. The 70-gene prognostic profile (van't Veer signature) [17] was used to divide the population into "Good prognosis" and "Poor prognosis" groups, and the histological classification was used to divide the tumors into "Triple negative" vs "Non triple-negative". The Beer Lung Metastasis Risk Index [13] was used to classify the tumors as Lung Metastasis Signature (LMS) Negative or Positive. The correlation between Rnd1 mRNA level and estrogen receptor (ER) status, tumor transcriptomic subtype or triple negative status was studied in 10 microarray data sets [13, 64–66]. Data were obtained from Oncomine [67]. Univariate survival analysis of Metastasis-Free Survival (MFS), Lung MFS and Bone MFS has been estimated according to the Kaplan-Meier method and analyzed by Log-rank (Mantel-Cox) and Gehan-Breslow-Wilcoxon Test. Hazard ratios and 95% confidence intervals (CIs) were calculated by use of a stratified Cox regression analysis. In the initial RhoGTPases screening, the patients' tumors were divided in two groups (low and high) on the basis of the median of all the values for the probesets for each RhoGTPase. For the survival analysis, 82 samples possessed complete clinical annotations and/or more than three years of clinical follow. Multivariate analysis was performed using the Cox proportional hazards model (R programming language). MCF10A cells were plated in triplicate at subconfluent density and infected with lentiviruses encoding sh-control or sh-Rnd1 (#1 and #2). cDNAs were hybridized to the Human HT-12 Expression BeadChip. Microarrays data analysis was performed with Partek Genomic Suite 6.4 software (Partek Inc., St.). Data were log2 transformed and normalized using scale to median. Principal Component Analysis (PCA) was used to verify the quality of data. Rnd1-regulated probesets consensually and significantly regulated by Rnd1 knock-down with a fold change (FC) ≥1.5 both in the comparison of either sh-#1 and sh-#2 versus scramble (total of 233 probesets) were used for hierarchical clustering and pathway analyses. A total of 233 genes (126 down-regulated and 117 up-regulated genes) were grouped in Biological Functions and Canonical Pathways by Ingenuity Pathway Analysis (IPA) Software (2009 Ingenuity Systems Inc). Only significantly regulated ($p \leq 0.05$, obtained by right-tailed Fisher Exact Test) pathways are shown. A subset of biologically interesting genes upregulated after Rnd1 silencing was selected for functional validation by qPCR (*CDC2*, *PLK1*, *CCNB2*, *CDCA1*).

Gene Set Enrichment Analysis

To examine if under-expression of RND1 correlates with activation of Ras, Myc, β-catenin or Src, we used oncogene signatures probe sets from primary human mammary epithelial cells transduced with oncogenic forms of the above signaling proteins [68]. Superman

correlations between the *RND1* probe and the oncogene signature probes were calculated for the MSKCC-99 (GSE-2603), EMC-286 (GES-2034), and EMC-192 (GSE-12276) dataset. These correlations were ranked and the ranks divided by total number to range it between 0 and 1. The ranks of the signature sets were used to calculate the CDF (cumulative distribution function) of the signature set ranks. If the ranks of the signature set are randomly distributed, the CDF will be along the diagonal. A departure from the diagonal indicates over or under representation. The correlation of low Rnd1 with activation of Ras signaling was confirmed by using an additional Ras signature [69].

FISH Analysis

To examine if *RND1* is inactivated by deletion in human breast cancer, we conducted 2-color FISH on 124 primary breast carcinomas from the Department of Pathology of the University of Torino using a probe spanning the RND1 locus located at Chr12q12-13 and a probe complementary to a centromeric sequence. Diagnoses were assigned according to the WHO classification by at least two experienced pathologists. Informed consents were obtained following the recommendations of local ethical committees (Protocol number 0081521 and 0072468). All locus-specific probes were developed using bacterial artificial chromosomes (BAC). The RP11-270J9 probe (CHORI), positioned centromeric (71 Kbp) to the RND1 gene and RP11-302B13 (CHORI) positioned telomeric (94 Kbp) to the RND1 gene were directly labeled with spectrum orange dUTP (Nick Translation Kit, Vysis Inc.). RP11-502N13 (CHORI), a control probe located on the p arm of chromosome 12, was labeled with spectrum green dUTP (Nick Translation Kit, Vysis Inc.). A probe specific for the centromeric region of chromosome 12 (Abbott Laboratories) was used to enumerate chromosome copy number. Probes and hybridization conditions were applied according to the Vysis manual instructions. Hybridization signals were analyzed using a fluorescent microscope (Olympus BX 51 Olympus America) or Zeiss AxioImage) with appropriate filters. Images were captured using the CytoVision imaging system (Applied Imaging) and/or analyzed using MetaSystem software. Tumor sections were first scanned at low power with a DAPI filter to identify areas of optimal tissue digestion and non-overlapping nuclei. Only intact nuclei were scored. The assay was considered positive for RND1 deletion if the signal revealed two green and one orange foci. The hybridization efficiency of the FISH probes was >95%, based on the hybridization signals in normal elements of cytological smears. At least one hundred nuclei per sample were analyzed and the highest number of tumor nuclei was collected for each individual slide. The neoplastic nuclei were defined based on cytological and histopathological features. Cutoff values for deletion were determined using 7 fibroadenoma breast tissues and 5 normal lymphoid tissues (tonsil and lymph nodes). Deletion-positive samples were defined when loss of RND1 signals was greater than 20% for paraffin-embedded tissue section of primary breast adenocarcinoma or of cell line paraffin embedded sections.

DNA Methylation Analysis

The methylation of the promoter region of *RND1* gene was examined by using the Epityper system from Sequenom (San Diego, CA). Specific PCR primers for bisulfite-converted DNA were designed using the EpiDesigner software (www.epidesigner.com). Primer

sequences, target chromosomal sequence, and Epityper specific tags are available upon request.

ChIP Assay

Chromatin immunoprecipitations were performed by using the ChIP assay kit from Millipore following standard protocols. The Rnd1 primers were as follows: Promoter Fwd-5′ CTCCAGCCTGACCTCACTTC and Rev-5′ CCCTTCCTCCCTTCTCTTTC; Intron Fwd-5′ TGCCCACTTCCAGTGAATTT and Rev-5′ TGTGATGGGAGGATCACTTG. GAPDH primers are from the kit.

Structural Analysis

The GTP loaded structure of RND1 was obtained form protein database PDB number 2CLS. The PyMOL program was used to predict and analyze the various mutational variants affecting effector loop and GTP loading.

SOLiD Sequencing

Analysis of TCGA datasets revealed that *RND1* suffers from point mutation in a small percentage of melanomas, colorectal carcinomas, endometrial carcinomas, and melanomas [54, 61]. The majority of the point mutations identified are likely to be pathogenic because they truncate Rnd1 (*A6fs*28*, *G70_splice*, *E162**, *Y164**, *R201**) or replace amino acid residues that are predicted to be necessary for its function (*E48K*, *D75N*, *S85L*, *W107G*, *R130Q*, and *L165P*). In addition, some individual mutations were identified in different tumor types (*D75N* and *R130Q*) and one patient tumor carried two missense mutations (*R130Q* and *A154T*). Since we only found one missense mutation in *RND*1 in breast cancer (*I217M*), we reasoned that the filters that had to be applied to these large datasets might have removed mutations present in a subpopulation of tumor cells. To examine if missense or nonsense mutations contribute to clonal inactivation of *RND1* in breast cancer, we divided 96 breast cancers from the University of Hiroshima in 10 pools and subjected them to targeted deep sequencing by SOLiD. Allelic variants present in the dbSNP137 database (>1,000 normal genomes) were excluded and putative pathogenic mutations were validated by SOLiD re-sequencing. Fresh frozen breast samples were obtained from the Department of Surgery of the University of Hiroshima following a protocol approved by the Institutional Review Board of the University. Informed consent was obtained for all samples. Genomic DNA samples extracted from 96 breast tumors and 8 normal breast tissues were amplified by PCR and the amplicons spanning the *RND1* exons from groups of 10 tumor samples or 8 normal breasts were pooled. 1 μg of pooled amplicons were concatenated, sheared for 5 minutes (covaris), end-repaired, and ligated with barcoded SOLiD sequencing adaptors. 8 cycles of PCR were performed and 2ng of the final 10 libraries were then pooled for one full size emulsion PCR using the EZbead system. The enriched beads were sequenced in an octet of a SOLiD4 sequencing system for 50 bp run with the Exact Call Chemistry module (ECC). An average of 6.2 million reads were generated per pool, the mapping rates ranged from 86.9% and 89.1%. The colorspace CSFASTA and QUAL files are first converted to double encoded FASTQ files which are then mapped to the target genome (hg19) using BWA (ver. 0.5.9-r16) with default options plus the color space mode option (-c) and the genome index

is built with the colorspace option. Variants were then called using a VarScan (ver 2.2) based pipeline. Reads for first filtered for those that had a MAPQ>40 (using samtools view –q 40) and also reads with undefined bases ('N') were removed. A pileup was generated with samtools mpileup with default depth set to 100,000 (-d 100000) and the resulting pileup was piped to varscan. Only variants in the *RND1* gene region were retained. Allelic variants present in the dbSNP 137 database (>1,000 normal genomes) were excluded and putative pathogenic mutations were validated by SOLiD re-sequencing. Informed consents were obtained and the protocol was approved by Internal Review Board (IRB) No. 299 from Hiroshima University.

Repeatability of experiments

All the results documented by immunoblots or micrographs are representative of experiments that were repeated independently at least twice with similar results. The number of independent experiments is specified in each figure legend and one representative experiment is shown.

Statistical analysis

Each experiment was repeated two or three times or more as mentioned in each figure legend. Data are presented as mean + S.D., unless stated otherwise. Student's *t*–test (unpaired, two-tailed) was used to compare two groups for independent samples. Meade's resource equation was used to predetermine sample size for primary tumor growth experiments (E:10–20). For lung colonization experiments, we used $n \geq 5$ unless because this sample size easily detects a large difference driven by a biologically robust event. No statistical method was used to predetermine sample size for in vitro experiments. Upon arrival mice were randomly allocated to experimental groups. Investigators were not blinded to allocation during experiments and outcome assessment.

Deposited data accession numbers

Following are the datasets generated for this study and deposited online.

MCF10A Rnd1 knockdown microarray: GSE43885

SOLiD sequencing data: GSE43828

Previously published datasets re-analyzed for this study

MSKCC-99: GSE-2603

EMC-286: GES-2034

EMC-192: GSE-12276

Supplementary Material

Refer to Web version on PubMed Central for supplementary material.

Acknowledgments

We thank Xuewu Zhang for advice, reagents, and for sharing the structure of the PlexinGAP-Rap1 complex prior to its publication. R.A. Weinberg, J.S. Brugge, M. Overholtzer, A. Ridley, B. Park, L. Tamagnome, M. Resh, H.

Djaballah, T. Kataoka, M. Negishi and D. Medina for reagents, K. Manova for assistance with confocal microscopy, R. Khanin and G.P. Gupta for help with multivariate analysis, and members of the Giancotti laboratory for discussions. We thank the Geoffrey Beene Translational Oncology Core, the Genomic Core, and the HTG Core of MSKCC for technical assistance. This work was supported by grants from the National Institutes of Health (P01 CA094060 Project 4 to F.G. and P30 CA08748 to MSKCC) and the Geoffrey Beene Cancer Center at MSKCC.

References

1. Collado M, Serrano M. Senescence in tumours: evidence from mice and humans. Nature reviews Cancer. 2010; 10:51–57.
2. Huang L, Muthuswamy SK. Polarity protein alterations in carcinoma: a focus on emerging roles for polarity regulators. Current opinion in genetics & development. 2010; 20:41–50. [PubMed: 20093003]
3. Thiery JP, Acloque H, Huang RY, Nieto MA. Epithelial-mesenchymal transitions in development and disease. Cell. 2009; 139:871–890. [PubMed: 19945376]
4. Ansieau S, et al. Induction of EMT by twist proteins as a collateral effect of tumor-promoting inactivation of premature senescence. Cancer cell. 2008; 14:79–89. [PubMed: 18598946]
5. Debnath J, et al. The role of apoptosis in creating and maintaining luminal space within normal and oncogene-expressing mammary acini. Cell. 2002; 111:29–40. [PubMed: 12372298]
6. Guo W, et al. Beta 4 integrin amplifies ErbB2 signaling to promote mammary tumorigenesis. Cell. 2006; 126:489–502. [PubMed: 16901783]
7. Dow LE, et al. Loss of human Scribble cooperates with H-Ras to promote cell invasion through deregulation of MAPK signalling. Oncogene. 2008; 27:5988–6001. [PubMed: 18641685]
8. Zhan L, et al. Deregulation of scribble promotes mammary tumorigenesis and reveals a role for cell polarity in carcinoma. Cell. 2008; 135:865–878. [PubMed: 19041750]
9. Yang J, et al. Twist, a master regulator of morphogenesis, plays an essential role in tumor metastasis. Cell. 2004; 117:927–939. [PubMed: 15210113]
10. Moody SE, et al. The transcriptional repressor Snail promotes mammary tumor recurrence. Cancer cell. 2005; 8:197–209. [PubMed: 16169465]
11. Jaffe AB, Hall A. Rho GTPases: biochemistry and biology. Annual review of cell and developmental biology. 2005; 21:247–269.
12. Sahai E, Marshall CJ. RHO-GTPases and cancer. Nature reviews Cancer. 2002; 2:133–142.
13. Minn AJ, et al. Genes that mediate breast cancer metastasis to lung. Nature. 2005; 436:518–524. [PubMed: 16049480]
14. Aguirre AJ, et al. High-resolution characterization of the pancreatic adenocarcinoma genome. Proceedings of the National Academy of Sciences of the United States of America. 2004; 101:9067–9072. [PubMed: 15199222]
15. Rutherford S, Hampton GM, Frierson HF, Moskaluk CA. Mapping of candidate tumor suppressor genes on chromosome 12 in adenoid cystic carcinoma. Laboratory investigation; a journal of technical methods and pathology. 2005; 85:1076–1085.
16. Yanagisawa M, et al. A p120 catenin isoform switch affects Rho activity, induces tumor cell invasion, and predicts metastatic disease. The Journal of biological chemistry. 2008; 283:18344–18354. [PubMed: 18407999]
17. van't Veer LJ, et al. Gene expression profiling predicts clinical outcome of breast cancer. Nature. 2002; 415:530–536. [PubMed: 11823860]
18. Gyorffy B, et al. An online survival analysis tool to rapidly assess the effect of 22,277 genes on breast cancer prognosis using microarray data of 1,809 patients. Breast cancer research and treatment. 2010; 123:725–731. [PubMed: 20020197]
19. Chardin P. Function and regulation of Rnd proteins. Nature reviews Molecular cell biology. 2006; 7:54–62.
20. Campisi J, d'Adda di Fagagna F. Cellular senescence: when bad things happen to good cells. Nature reviews Molecular cell biology. 2007; 8:729–740.
21. Luo J, et al. A genome-wide RNAi screen identifies multiple synthetic lethal interactions with the Ras oncogene. Cell. 2009; 137:835–848. [PubMed: 19490893]

22. Jonsson G, et al. High-resolution genomic profiles of breast cancer cell lines assessed by tiling BAC array comparative genomic hybridization. Genes, chromosomes & cancer. 2007; 46:543–558. [PubMed: 17334996]
23. Bretones G, et al. SKP2 oncogene is a direct MYC target gene and MYC down-regulates p27(KIP1) through SKP2 in human leukemia cells. The Journal of biological chemistry. 2011; 286:9815–9825. [PubMed: 21245140]
24. Elenbaas B, et al. Human breast cancer cells generated by oncogenic transformation of primary mammary epithelial cells. Genes & development. 2001; 15:50–65. [PubMed: 11156605]
25. Podsypanina K, Politi K, Beverly LJ, Varmus HE. Oncogene cooperation in tumor maintenance and tumor recurrence in mouse mammary tumors induced by Myc and mutant Kras. Proceedings of the National Academy of Sciences of the United States of America. 2008; 105:5242–5247. [PubMed: 18356293]
26. Courtois-Cox S, et al. A negative feedback signaling network underlies oncogene-induced senescence. Cancer cell. 2006; 10:459–472. [PubMed: 17157787]
27. Cichowski K, Santiago S, Jardim M, Johnson BW, Jacks T. Dynamic regulation of the Ras pathway via proteolysis of the NF1 tumor suppressor. Genes & development. 2003; 17:449–454. [PubMed: 12600938]
28. McCormack J, Welsh NJ, Braga VM. Cycling around cell-cell adhesion with Rho GTPase regulators. Journal of cell science. 2013; 126:379–391. [PubMed: 23547086]
29. Shin S, Dimitri CA, Yoon SO, Dowdle W, Blenis J. ERK2 but not ERK1 induces epithelial-to-mesenchymal transformation via DEF motif-dependent signaling events. Molecular cell. 2010; 38:114–127. [PubMed: 20385094]
30. Wennerberg K, et al. Rnd proteins function as RhoA antagonists by activating p190 RhoGAP. Current biology: CB. 2003; 13:1106–1115. [PubMed: 12842009]
31. Oinuma I, Ishikawa Y, Katoh H, Negishi M. The Semaphorin 4D receptor Plexin-B1 is a GTPase activating protein for R-Ras. Science. 2004; 305:862–865. [PubMed: 15297673]
32. Tamagnone L. Emerging role of semaphorins as major regulatory signals and potential therapeutic targets in cancer. Cancer cell. 2012; 22:145–152. [PubMed: 22897846]
33. Giordano S, et al. The semaphorin 4D receptor controls invasive growth by coupling with Met. Nature cell biology. 2002; 4:720–724.
34. Swiercz JM, Kuner R, Offermanns S. Plexin-B1/RhoGEF-mediated RhoA activation involves the receptor tyrosine kinase ErbB-2. The Journal of cell biology. 2004; 165:869–880. [PubMed: 15210733]
35. Wang Y, et al. Plexins are GTPase-activating proteins for Rap and are activated by induced dimerization. Science signaling. 2012; 5:ra6. [PubMed: 22253263]
36. Wang Y, Pascoe HG, Brautigam CA, He H, Zhang X. Structural basis for activation and non-canonical catalysis of the Rap GTPase activating protein domain of plexin. eLife. 2013; 2:e01279. [PubMed: 24137545]
37. Frech M, et al. Inhibition of GTPase activating protein stimulation of Ras-p21 GTPase by the Krev-1 gene product. Science. 1990; 249:169–171. [PubMed: 2164710]
38. Hata Y, et al. Inhibition of the ras p21 GTPase-activating protein-stimulated GTPase activity of c-Ha-ras p21 by smg p21 having the same putative effector domain as ras p21s. The Journal of biological chemistry. 1990; 265:7104–7107. [PubMed: 2158984]
39. Danielson KG, Oborn CJ, Durban EM, Butel JS, Medina D. Epithelial mouse mammary cell line exhibiting normal morphogenesis in vivo and functional differentiation in vitro. Proceedings of the National Academy of Sciences of the United States of America. 1984; 81:3756–3760. [PubMed: 6587390]
40. Barcellos-Hoff MH, Ravani SA. Irradiated mammary gland stroma promotes the expression of tumorigenic potential by unirradiated epithelial cells. Cancer research. 2000; 60:1254–1260. [PubMed: 10728684]
41. Giancotti FG. Mechanisms governing metastatic dormancy and reactivation. Cell. 2013; 155:750–764. [PubMed: 24209616]

42. Yao J, et al. Combined cDNA array comparative genomic hybridization and serial analysis of gene expression analysis of breast tumor progression. Cancer research. 2006; 66:4065–4078. [PubMed: 16618726]
43. Sakai W, et al. Secondary mutations as a mechanism of cisplatin resistance in BRCA2-mutated cancers. Nature. 2008; 451:1116–1120. [PubMed: 18264087]
44. Tan J, et al. Pharmacologic disruption of Polycomb-repressive complex 2-mediated gene repression selectively induces apoptosis in cancer cells. Genes & development. 2007; 21:1050–1063. [PubMed: 17437993]
45. Bell CH, Aricescu AR, Jones EY, Siebold C. A dual binding mode for RhoGTPases in plexin signalling. PLoS biology. 2011; 9:e1001134. [PubMed: 21912513]
46. Ahearn IM, Haigis K, Bar-Sagi D, Philips MR. Regulating the regulator: post-translational modification of RAS. Nature reviews Molecular cell biology. 2012; 13:39–51.
47. Hydbring P, et al. Phosphorylation by Cdk2 is required for Myc to repress Ras-induced senescence in cotransformation. Proceedings of the National Academy of Sciences of the United States of America. 2010; 107:58–63. [PubMed: 19966300]
48. Serrano M, Lin AW, McCurrach ME, Beach D, Lowe SW. Oncogenic ras provokes premature cell senescence associated with accumulation of p53 and p16INK4a. Cell. 1997; 88:593–602. [PubMed: 9054499]
49. Ohtsuka T, Shimizu K, Yamamori B, Kuroda S, Takai Y. Activation of brain B-Raf protein kinase by Rap1B small GTP-binding protein. The Journal of biological chemistry. 1996; 271:1258–1261. [PubMed: 8576107]
50. Vossler MR, et al. cAMP activates MAP kinase and Elk-1 through a B-Raf- and Rap1-dependent pathway. Cell. 1997; 89:73–82. [PubMed: 9094716]
51. York RD, et al. Rap1 mediates sustained MAP kinase activation induced by nerve growth factor. Nature. 1998; 392:622–626. [PubMed: 9560161]
52. Mishra S, Smolik SM, Forte MA, Stork PJ. Ras-independent activation of ERK signaling via the torso receptor tyrosine kinase is mediated by Rap1. Current biology: CB. 2005; 15:366–370. [PubMed: 15723799]
53. Itoh M, Nelson CM, Myers CA, Bissell MJ. Rap1 integrates tissue polarity, lumen formation, and tumorigenic potential in human breast epithelial cells. Cancer research. 2007; 67:4759–4766. [PubMed: 17510404]
54. Forbes SA, et al. COSMIC (the Catalogue of Somatic Mutations in Cancer): a resource to investigate acquired mutations in human cancer. Nucleic acids research. 2010; 38:D652–657. [PubMed: 19906727]
55. Eckert LB, et al. Involvement of Ras activation in human breast cancer cell signaling, invasion, and anoikis. Cancer research. 2004; 64:4585–4592. [PubMed: 15231670]
56. Rody A, et al. Poor outcome in estrogen receptor-positive breast cancers predicted by loss of plexin B1. Clinical cancer research: an official journal of the American Association for Cancer Research. 2007; 13:1115–1122. [PubMed: 17317819]
57. Argast GM, et al. Plexin B1 is repressed by oncogenic B-Raf signaling and functions as a tumor suppressor in melanoma cells. Oncogene. 2009; 28:2697–2709. [PubMed: 19483722]
58. Wong OG, et al. Plexin-B1 mutations in prostate cancer. Proceedings of the National Academy of Sciences of the United States of America. 2007; 104:19040–19045. [PubMed: 18024597]
59. Banerji S, et al. Sequence analysis of mutations and translocations across breast cancer subtypes. Nature. 2012; 486:405–409. [PubMed: 22722202]
60. Tong Y, Hota PK, Hamaneh MB, Buck M. Insights into oncogenic mutations of plexin-B1 based on the solution structure of the Rho GTPase binding domain. Structure. 2008; 16:246–258. [PubMed: 18275816]
61. Gao J, et al. Integrative analysis of complex cancer genomics and clinical profiles using the cBioPortal. Science signaling. 2013; 6:pl1. [PubMed: 23550210]
62. Neve RM, et al. A collection of breast cancer cell lines for the study of functionally distinct cancer subtypes. Cancer cell. 2006; 10:515–527. [PubMed: 17157791]

63. Debnath J, Muthuswamy SK, Brugge JS. Morphogenesis and oncogenesis of MCF-10A mammary epithelial acini grown in three-dimensional basement membrane cultures. Methods. 2003; 30:256–268. [PubMed: 12798140]

64. Richardson AL, et al. X chromosomal abnormalities in basal-like human breast cancer. Cancer cell. 2006; 9:121–132. [PubMed: 16473279]

65. Chin K, et al. Genomic and transcriptional aberrations linked to breast cancer pathophysiologies. Cancer cell. 2006; 10:529–541. [PubMed: 17157792]

66. Lu X, et al. Predicting features of breast cancer with gene expression patterns. Breast cancer research and treatment. 2008; 108:191–201. [PubMed: 18297396]

67. Rhodes DR, et al. ONCOMINE: a cancer microarray database and integrated data-mining platform. Neoplasia. 2004; 6:1–6. [PubMed: 15068665]

68. Bild AH, et al. Oncogenic pathway signatures in human cancers as a guide to targeted therapies. Nature. 2006; 439:353–357. [PubMed: 16273092]

69. Sweet-Cordero A, et al. An oncogenic KRAS2 expression signature identified by cross-species gene-expression analysis. Nature genetics. 2005; 37:48–55. [PubMed: 15608639]

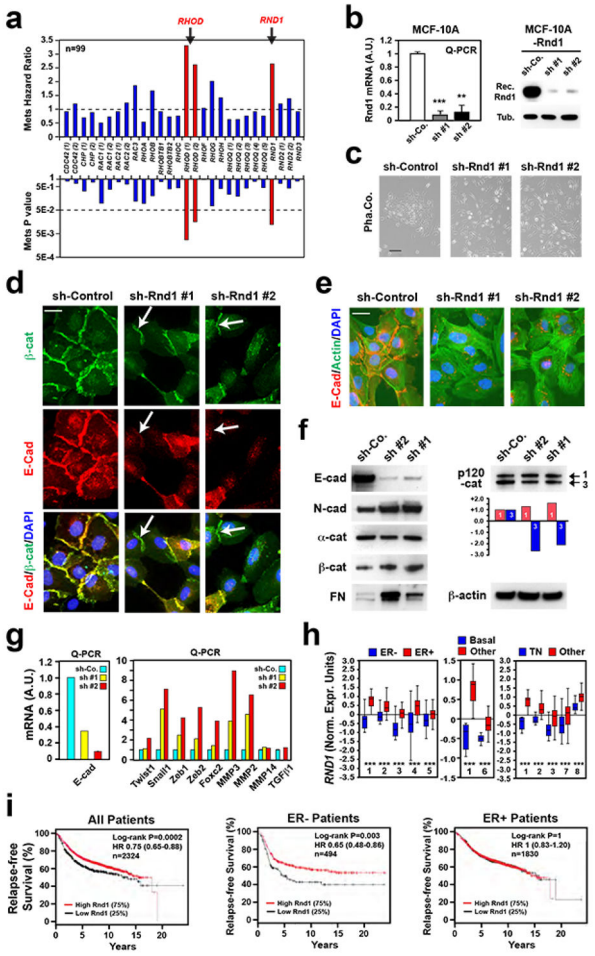

Figure 1.

Identification of *RND1* as a candidate breast tumor suppressor. (**a**) Kaplan-Meier analysis of the correlation between the level of the mRNA encoding each Rho-family GTPase and Metastasis-Free Survival (MFS) in the MSKCC data set. The graph shows the hazard ratio (top) and the Log-rank P value (bottom) associated with expression of each Rho GTPase. (**b**) MCF-10A cells were transduced with lentiviral vectors encoding two shRNAs targeting Rnd1 or a control shRNA and subjected to Q-PCR for Rnd1 (left) or infected with a retrovirus encoding wild-type Rnd1 followed by lentiviruses carrying two shRNAs targeting Rnd1 or a control sh-RNA and subjected to immunoblotting with affinity-purified antibody to Rnd1 (right). See Methods for the antibodies. The graph shows the average and SD (*n*=3 biological replicates). (**c–g**) Control and Rnd1-silenced MCF-10A cells were cultured for 5 days and photographed; Scale bar, 50 μm (c) or they were subjected to immunofluorescent staining for β-catenin (β-cat, Green), E-cadherin (E-Cad, Red) and DAPI (d) or anti-E-cadherin (E-Cad, Red), Phalloidin (Actin, Green) and DAPI (e). Pictures show areas of similar cell density. Scale bars are 15 μM. (**f**) Control and Rnd1-silenced MCF-10A cells were subjected to immunoblotting with the indicated antibodies. Arrows point to the mesenchymal (1) and epithelial (3) splice isoform of p120 catenin. The graph shows a densitometric quantification of the abundance of isoforms as fold change over control

values. (**g**) Control and Rnd1-silenced MCF-10A cells were subjected to Q-PCR for the indicated genes. Data are from one experiment in which triplicate samples were assessed in parallel (*n*=2 biological replicates). (**h**) Correlation between normalized *RND1* mRNA levels and Estrogen Receptor (ER) status (left) and transcriptomic tumor subtypes (middle and right) in breast cancer DNA microarray data sets available from Oncomine (1: Richardson; n=47, 2: Chin; n=118, 3: Minn; n=121, 4: Lu; n=129, 5: Wang; n=286, 6: Ginestier; n=55, 7: Farmer; n=49, 8: Hess; n=133). n= number of patients. Box represents median values. (**i**) Kaplan-Meier analysis of relapse-free survival for all patients (n=2324), ER-negative patients (n=494), or ER-positive patients (n=1830) using the open source KM Plotter (http://kmplot.com/analysis). Panels c, d, e, and f show one representative experiment (*n*=3). P values by the Student's *t*-test are: *, P=<0.05; **, P=<0.01; ***, P<0.001. The biological replicates yielded similar results. For source data, see Supplementary Table 8. Uncropped blots are shown in Supplementary Fig. 9.

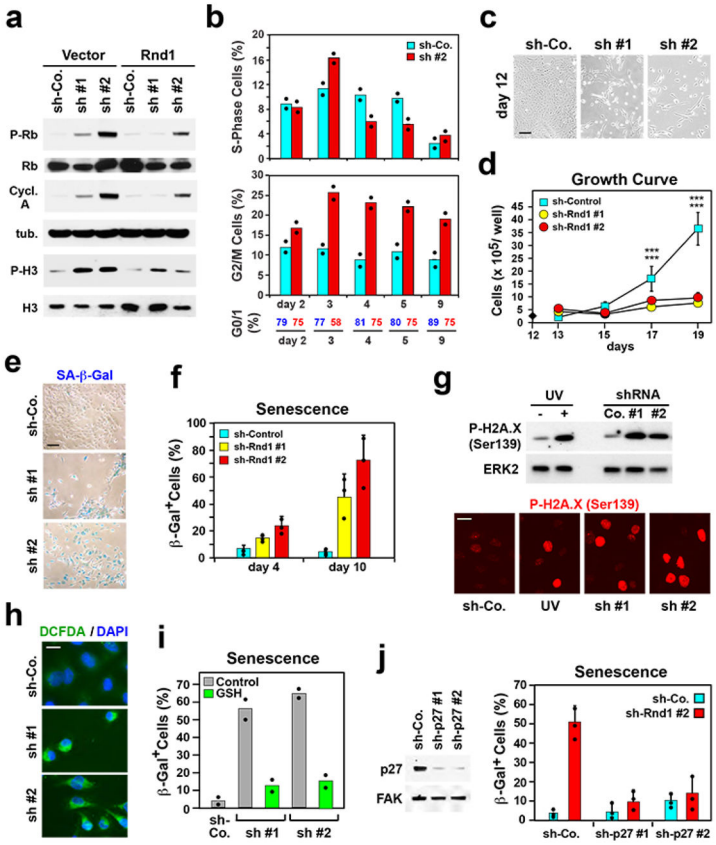

Figure 2.

Depletion of Rnd1 causes hyperproliferative stress followed by premature senescence. (**a**) MCF-10A cells transduced with Rnd1 or control vector were infected with lentiviruses carrying either control shRNA or 2 shRNAs targeting Rnd1, and 2 days later subjected to immunoblotting with the indicated antibodies. (**b**) MCF-10A cells infected with either control shRNA or shRNA targeting Rnd1 (sh #2) were subjected to Propidium Iodide staining and FACS analysis. The graphs show the percentage of cells in S-phase (top) and G2/M-phase (bottom). The percentage of cells in G0/G1-phase is indicated below the graphs. Data from one experiment are shown as averages of two technical replicates (n=2 biological replicates). (**c**) After transduction, control and Rnd1-silenced MCF-10A cells were passaged twice, cultured for 3 additional days, and photographed (total 12 days). Scale bar, 50 μm. (**d**) One day later, equal numbers of cells from (c) were plated and subjected to growth assay. The graph shows the average and SD from 3 independent experiments, each conducted in triplicate plates (n=3 biological replicates). *** represents P<0.001 by the Student's t-test. (**e**) Control and Rnd1-silenced MCF-10A cells were subjected to Senescent Associated (SA)-β-galactosidase staining. Scale bar, 50 μm. (**f**) The graph shows the percentage of SA-β-galactosidase-positive cells at the indicated times. Individual data points, their average and SD are from one experiment in which triplicate samples were assessed in parallel (n=3 biological replicates). (**g**) MCF-10A cells were exposed to UV (100 Joules/cm^2) or left untreated or they were transduced as indicated and cultured for 4 days prior to immunoblotting (top) or immunofluorescent staining (bottom). Scale bar, 15 μm. (**h**)

Control and Rnd1-silenced MCF-10A cells were incubated with H_2DCFDA to detect reactive oxygen species (Green) and DAPI (blue). Scale bar, 15 μm. (**i**) MCF-10A cells infected as above were cultured with or without 0.5 mM reduced Glutathione (GSH) for 24 hours and subjected to staining for Senescent Associated (SA)-β-galactosidase activity. Individual data points, their average and SD are from one experiment in which duplicate samples were assessed in parallel (*n*=2 biological replicates). (**j**) MCF-10A cells were infected with control shRNA or shRNAs targeting p27 and subjected to immunoblotting (left). The p27-silenced cells were infected with control or Rnd1 shRNA (#2) and subjected to SA-β-galactosidase staining. The graph shows the percentage of SA-β-galactosidase-positive cells after 10 days (right). Individual data points, their average and SD are from one experiment in which triplicate samples were assessed in parallel (*n*=2 biological replicates). Panels a, g and h show one representative experiment out of two while panels c and e of three performed. The biological replicates of b, f, i, and j yielded similar results. For source data see Supplement Table 8 Uncropped blots are shown in Supplementary Fig. 9.

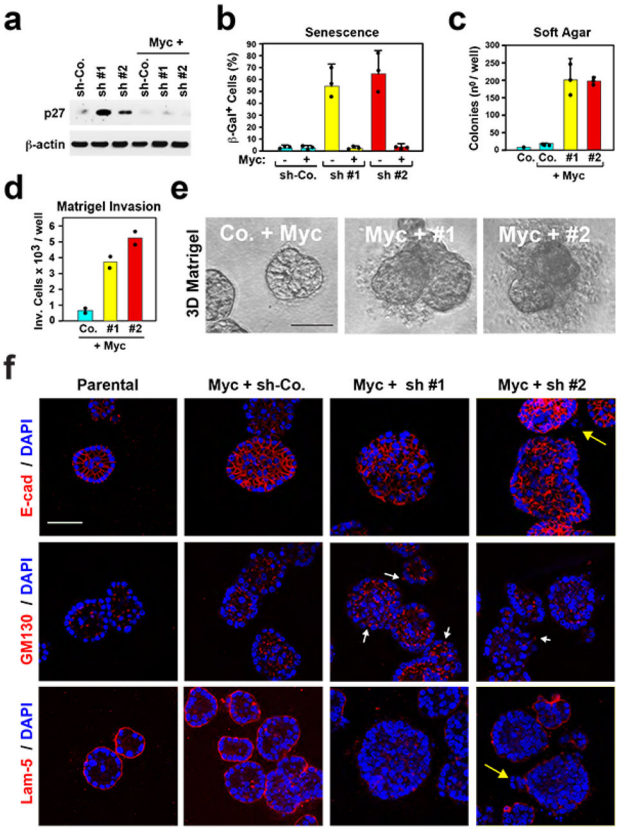

Figure 3.

Inactivation of Rnd1 induces hyperproliferation and invasion in 3D Matrigel. (**a–b**) MCF-10A cells were transduced or not with Myc, infected with either control shRNA or two shRNAs targeting Rnd1, cultured for 9 days and subjected to immunoblotting with antibodies to p27 and β-actin (a) or cultured for 4 additional days and subjected to SA-β-Galactosidase staining. The graph shows the individual data points, their average, and SD from one experiment in which triplicate samples were assessed in parallel (*n*=2 biological replicates). See representative images in Supplementary Figure S3e (b). (**c**) MCF-10A cells were transduced or not with Myc, infected with either control shRNA or two shRNAs targeting Rnd1, cultured for 12 days, and subjected to soft agar assay. The graph shows the individual data points, their average, and SD from one experiment performed in triplicate and accessed in parallel (*n*=3 biological replicates). (**d**) The indicated cells were subjected to Matrigel invasion assay and the graph indicates the number of cells invaded per well in each group. Data are from one representative experiment shown as averages of two technical repeats (*n*=3 biological replicates). (**e**) MCF-10A cell expressing Myc were infected with control shRNA or two shRNAs targeting Rnd1 and cultured in 3D Matrigel for 8 days. The pictures show representative phase-contrast images of pseudoacinar structures. Scale bars are 50 μm. (**f**) Parental MCF-10A cells and MCF-10A cells expressing Myc were infected as indicated above, cultured in 3D Matrigel for 8 days, and subjected to immunofluorescent staining with the indicated antibodies followed by DAPI. The long yellow arrows in the top and bottom panel of the right column show a group of cells invading through a discontinuity

of the basement membrane. The small white arrows in the two panels of the central column show cells that have lost their apical positioning of the Golgi apparatus. Scale bars are 50 μM. Panels a, e, and f show the results of one representative experiment out of three performed independently. The biological repeats of b-d yielded similar results. For source data, see Supplementary Table 8. Uncropped blots are shown in Supplementary Fig. 9.

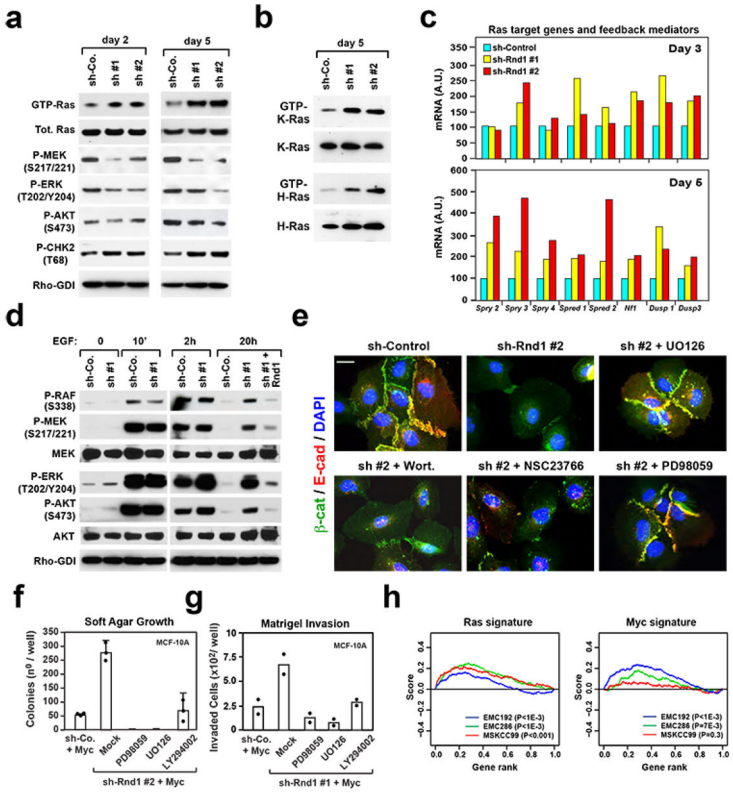

Figure 4.

Loss of Rnd1 activates oncogenic Ras signaling. (**a**) MCF10A cells infected with a control or 2 sh-RNAs targeting Rnd1 were deprived of growth factors for 24 hours at the indicated times after infection and subjected to pull-down assay using GST-RBD and immunoblotting with the indicated antibodies. (**b**) MCF-10A cells were infected as above, cultured for 5 days and subjected to pull-down assay using GST-RBD followed by immunoblotting with antibodies to K-Ras or H-Ras. (**c**) MCF-10A cells were infected as above, cultured for 3 (top) or 5 days (bottom) and subjected to Q-PCR for the indicated genes. Values represent fold change from one representative experiment (*n*=2 biological replicates). (**d**) MCF-10A cells expressing a control shRNA (sh-Co.) and spontaneously immortalized Rnd1-silenced MCF-10A cells (sh #1) were deprived of growth factors for 24 hours, stimulated with EGF (5 ng/ml) for the indicated times and subjected to immunoblotting as indicated. As a control, spontaneously immortalized Rnd1-silenced cells were re-infected with a retroviral vector encoding Rnd1 (sh #1 + Rnd1), deprived of growth factors, stimulated with EGF for 20 hours, and analyzed as above. (**e**) Four days after infection with a control shRNA or two shRNAs targeting Rnd1, MCF-10A cells were cultured for 24 hours with U0126 and PD98059 (MEK inhibitors), Wortmannin (PI3K inhibitor) or NSC23766 (Rac inhibitor). Cells were subjected to immunofluorescent staining as indicated. Scale bar, 15 μM. (**f, g**) MCF-10A cells expressing Myc were infected with a control shRNA (sh-Co. + Myc) or one targeting Rnd1 (sh-Rnd1 + Myc) and subjected to soft agar assay (f) or Matrigel invasion assay (g) in the presence of the indicated inhibitors. Data in f are from one experiment and are shown as averages and SD of three technical replicates (*n*=2 biological replicates). Data

in g are from one experiment and are shown as averages of two technical replicates (*n*=2 biological replicates). (**h**) Gene set enrichment analysis plots showing that low *RND1* mRNA levels are inversely correlated with the expression of a Ras and a Myc signature. See methods for details. Panels a, b, d, and e show one representative experiment out of three performed independently. The biological replicates of c, f, and g yielded similar results. For source data, see Supplementary Table 8. Uncropped blots are shown in Supplementary Fig. 9.

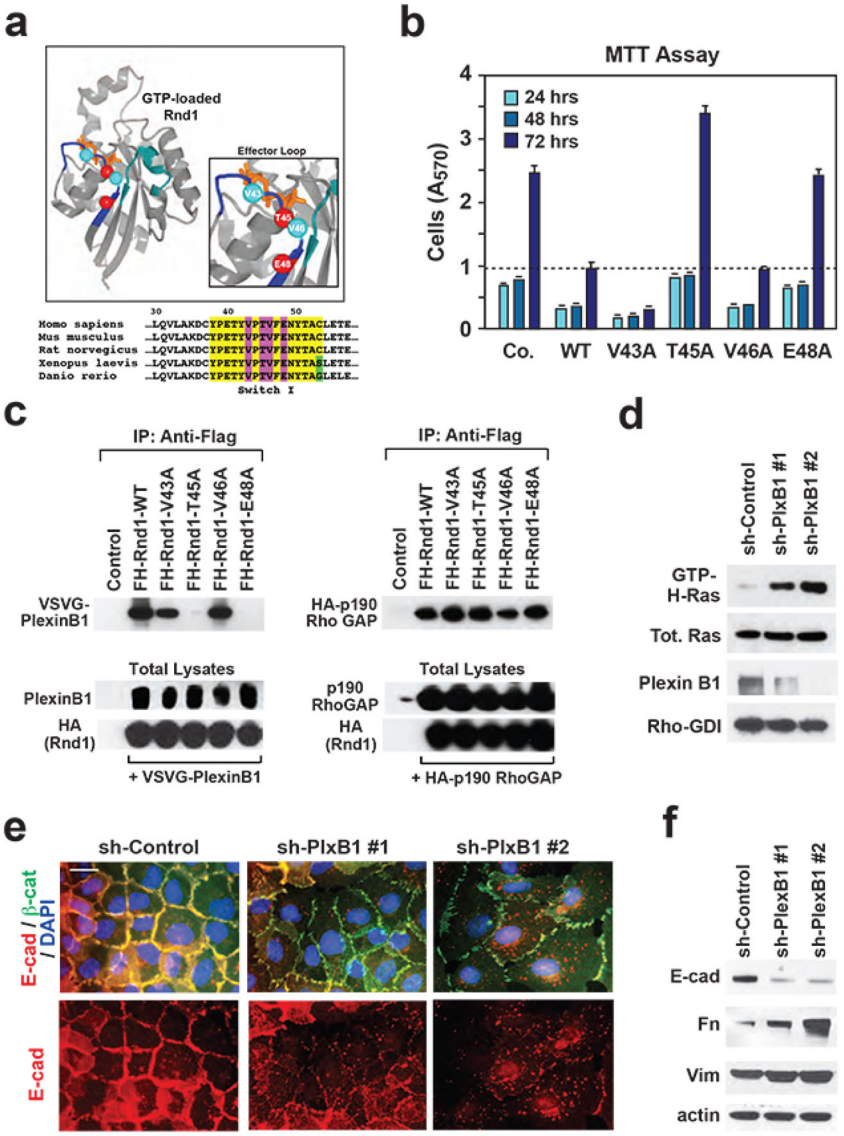

Figure 5.

Rnd1 suppresses activation of Ras and EMT by binding to Plexin B1. (**a**) Structure of GTP-loaded Rnd1. Switch I and II regions are depicted in blue and cyan, respectively. GTP is in orange. Mutated residues resulting in loss of function are shown as red balls, non-functional mutations as pale blue balls. (**b**) MCF-10A cells were infected with a retrovirus encoding HA-tagged wild type or mutant Rnd1 or empty vector (Co.), plated under sparse conditions and subjected to MTT assay at the indicated times. Data are shown as averages and SD of 6 technical replicates (*n*=2 biological replicates). (**c**) HEK293T cells were transfected with a vector encoding Flag-HA-tagged versions of wild type or mutant RND1 or with empty vector together with a vector encoding VSVG-PlexinB1 or a vector encoding HA-p190RhoGAP. Total lysates were subjected to immunoprecipitation with anti-Flag antibody followed by immunoblotting with VSVG-PlexinB1 (left) and HA-p190RhoGap (right). (**d**) MCF10A cells were infected with lentiviruses carrying either a control shRNA (sh-Co.) or 2

sh-RNA targeting PlexinB1 (sh-PlxB1 #1 and #2). Total lysates were immunoblotted as indicated or subjected to pull down assay using GST-RBD. Data are representative of two independent experiments. (**e**) PlexinB1 knockdown MCF10A cells were subjected to immunofluorescent staining with antibodies as indicated followed by DAPI staining. Scale bar is 15 μM. (**f**) The above lysates were immunoblotted with antibodies to the indicated EMT markers. Panels c–f show one representative experiment out of three performed independently. The biological repeat of b yielded similar results. For source data, see Supplementary Table 8. Uncropped images of blots are shown in Supplementary Fig. 9.

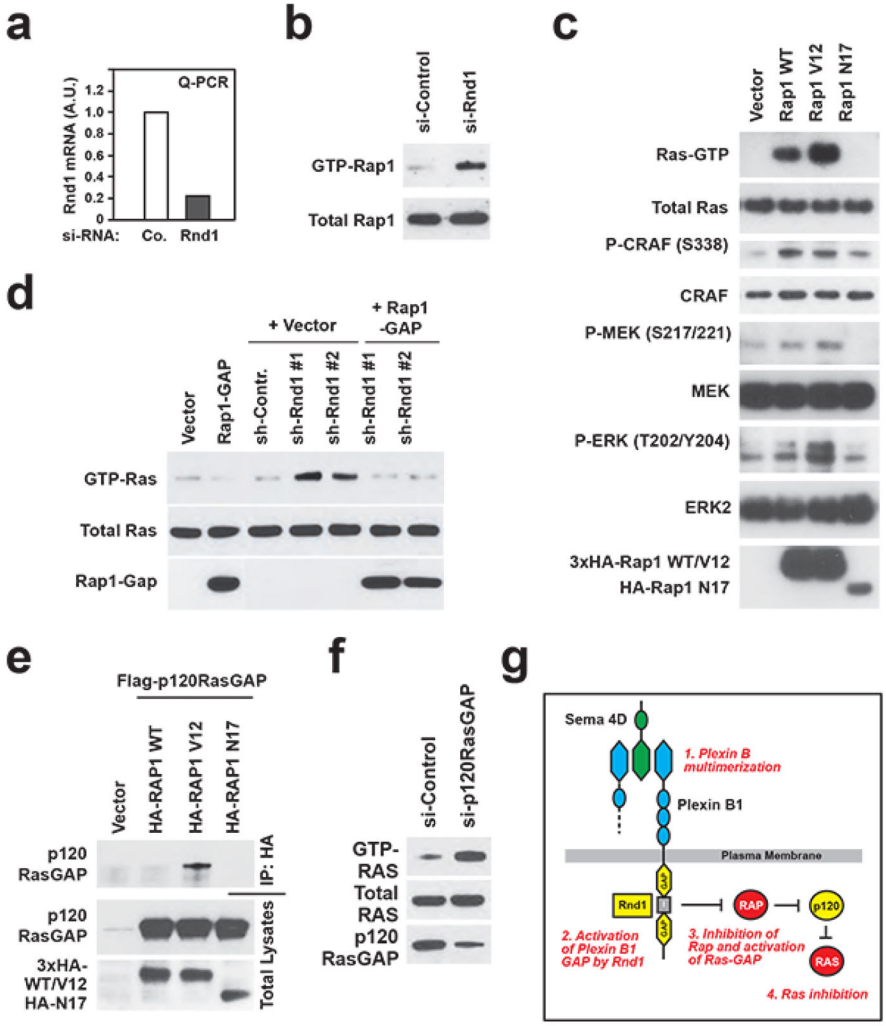

Figure 6.

Loss of Rnd1 activates Rap1 and inhibits p120Ras GTPase activity. (**a, b**) MCF-10A cells were transfected with either control siRNA or Rnd1 specific siRNA, cultured for 3 days and subjected to Q-PCR (*n*=2 biological replicates) (a) or pull-down assay using GST-RID to detect activated Rap1 (b). (**c**) 293T cells were transfected with empty vector and plasmids encoding wild type Rap1, constitutively active Rap1-V12 and dominant negative Rap1-N17. Cell lysates were subjected to GST-RBD pull down assay followed by immunoblotting with anti-Ras (top blot) or immunoblotted as indicated (bottom blots). (**d**) MCF-10A cells were infected with a control shRNA or 2 shRNAs targeting Rnd1 and, after 36 hours, re-infected with an empty vector or one expressing Rap1GAP. Cells were deprived of growth factors for 24 hours and subjected to pull-down assay using GST-RBD to detect activated Ras. Control MCF-10A cells were infected with empty vector or one expressing Rap1-GAP and collected at 36 hours post infection. (**e**) 293T cells were transfected with a Flag-tagged form of p120RasGap together with HA-tagged Rap1-WT, Rap1-V12 or Rap1-N17. Total lysates were subjected to immunoprecipitation with anti-HA followed by immunoblotting with anti-p120RasGap. Cells transfected with empty vector were used as control. (**f**) MCF-10A cells

were transfected with control si-RNA or si-RNA targeting p120RasGap and total lysates were subjected to GST-RBD pull down assay to detect activated Ras. (**g**) Mechanistic model showing Rnd1 dependent regulation of Ras activation through Rap mediated interaction of p120RasGap. Panels c, d, and e show one representative experiment out of three performed. The experiments in b and f were performed two times with similar results. For source data, see Supplementary Table 8. Uncropped images of blots are shown in Supplementary Fig. 9.

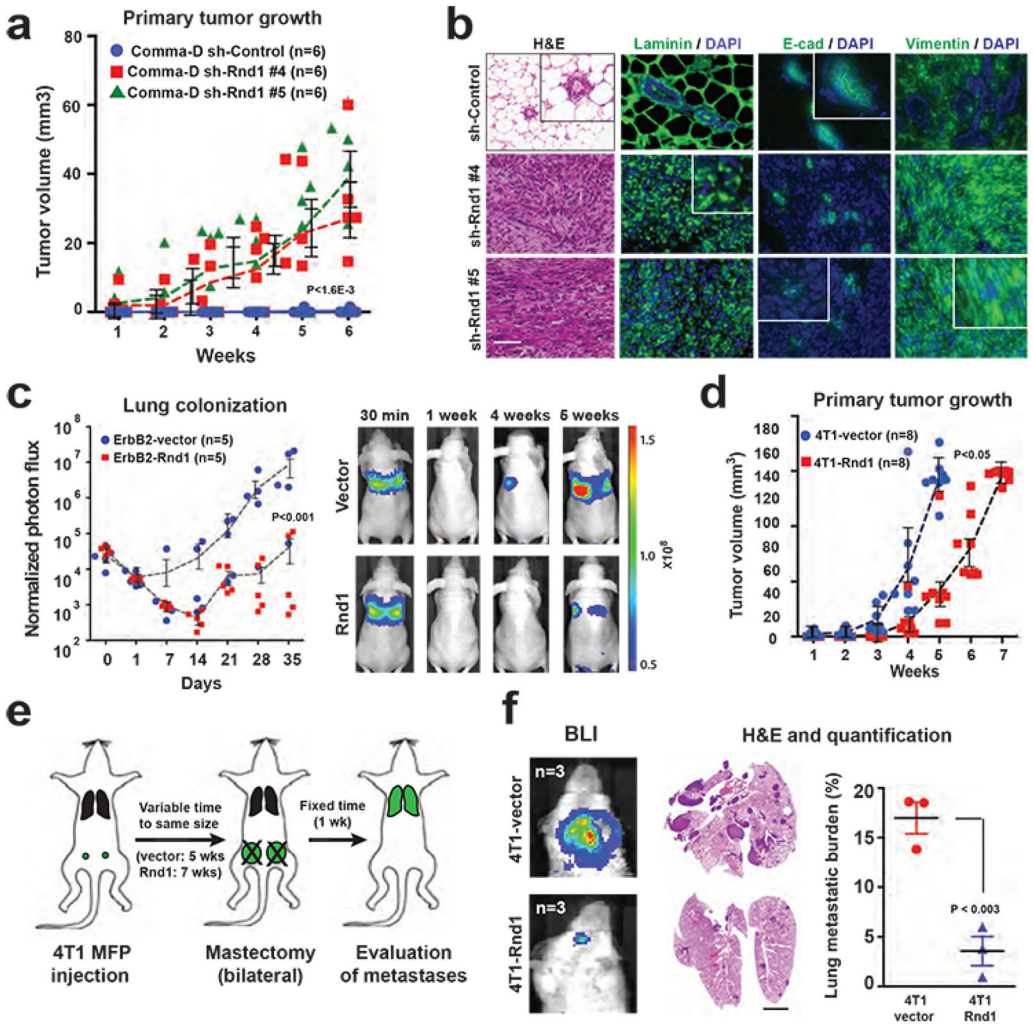

Figure 7.

Loss of Rnd1 initiates mammary tumorigenesis. (**a**) Comma-D cells were infected with lentiviruses carrying a control shRNA or two shRNAs targeting Rnd1. Cells (1×10^6) were injected into the fourth mammary fat pad of NOD-SCID-γ (NSG) mice. Tumor growth was measured at the indicated times using a caliper. The graph shows individual data points for tumor volumes, their average and SEM from *n*=6 tumors per group. (**b**) Comma-D derived tumors carrying the indicated constructs were sectioned and subjected to immunofluorescent staining with antibodies to total Laminin, E-cadherin, or Vimentin followed by DAPI. Scale bars are 50 μM. (**c**) ErbB2 transformed mammary tumor cells from MMTV-Neu (YD) mice infected with retroviral vector encoding HA-RND1 or a control vector and labeled with TGL were inoculated intravenously via tail vein into nude mice (*n*=5 mice per group). Lung colonization was measured by bioluminescent imaging (left). Data represents normalized photon flux at the indicated time points for each mouse. Representative images of one mouse are shown (right). (**d**) 4T1-TGL cells (1×10^3) were injected bilaterally into the fourth mammary fat pad of Balb/C mice and monitored for tumor growth. Data points represent tumor volumes in cubic millimeters at the indicated time points for each mouse in

two cohorts of mice: one infected with retroviral vector encoding HA-RND1 (red squares) and second with a control vector (blue circles). *n*=8 tumors per group. (**e**) Schematic representation of the spontaneous metastasis experiment. (**f**) Representative images from the experiment showing lung bioluminescence at 1 week after mastectomy (left) and H&E-stained lung sections (middle). *n*= 3 lungs in each cohort. The graph shows the lung metastatic burden in mice injected with control and Rnd1-expressing 4T1 cells (right). Scale bar is 1 mm. The experiments in a, c, and d were performed two times with similar results, whereas that in f was performed once. Error bars are SEM and *P* values were calculated by using the Student's *t*-test. For source data, see Supplementary Table 8.

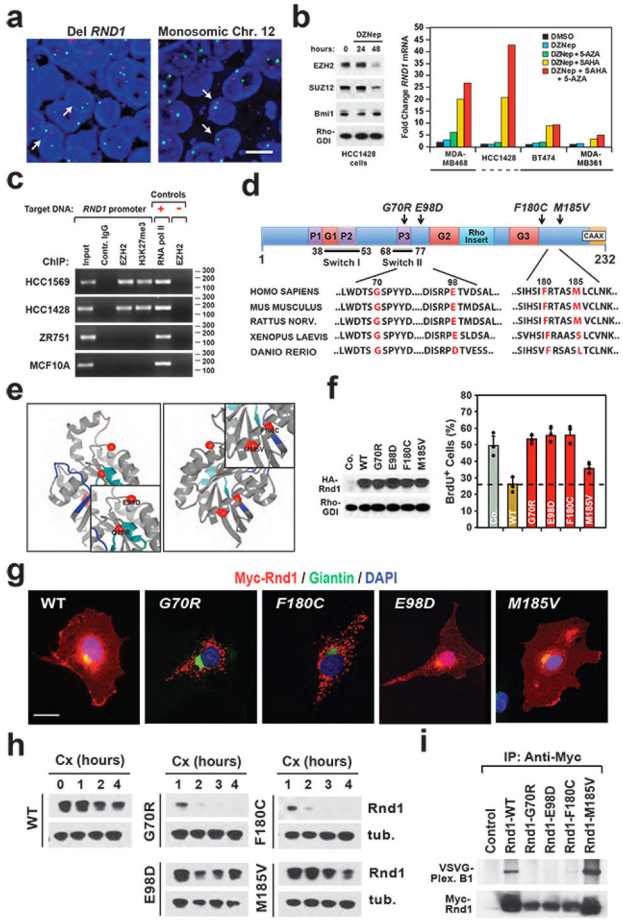

Figure 8.

Genetic and epigenetic inactivation of *RND1* in human breast cancer. (**a**) Representative images of breast cancer sections hybridized with a centromeric 12 chromosome (green) and locus-specific *RND1* (red, RP11-270J9) probe. Left panel: *RND1* deletion (single red dot); right panel: 12 chr. monosomic deletion. Scale bar, 20 μm. (**b**) HCC1428 cells treated with DZNep (5 μM) were immunoblotted with the antibodies indicated (left). Human breast cancer cell lines were treated with DZNep in combination with either 5-AZA (10 μM), SAHA (5 μM), or both and *Rnd1* transcript was assessed by Q-PCR. Data are from one experiment shown as averages of three technical replicates (n=2 biological replicates). (**c**) ChIP assay of the *RND1* promoter with antibodies to EZH2, H3K27me3, or control RNA pol II and IgG, as indicated. Sequences from the *GAPDH* promoter and a *RND1* intron were used as positive (+) and negative (−) controls, respectively. (**d**) Schematic representation showing the domain organization of Rnd1. Arrows point to the position of tumor-derived mutations. The amino acid sequences surrounding mutated residues (red) from various species are aligned below. **(e)** Crystal structure of Rnd1 and insets show magnifications of relevant regions. Tumor-derived mutation residues are depicted as red balls. Switch I and II segments are depicted in blue and cyan, respectively. (**f**) MCF-10A cells expressing HA-tagged wild type or mutant RND1 proteins or empty vector (Co.) were deprived of growth factors and subjected to BrdU incorporation assay. Data are averages of three technical

replicates from one experiment (*n*=2 biological replicates). Error bars are SD (top). Immunoblotting shows the expression of HA-Rnd1 (bottom). (**g**) HUVEC cells were transfected with Myc-tagged forms of Rnd1 and subjected to immunofluorescent staining with anti-Myc (Red), Giantin (Green) and DAPI (Blue). Scale bars are 15 μM. (**h**) 293T cells transfected with Myc-tagged Rnd1 were treated with Cycloheximide (75 μg/ml) and immunoblotted with anti-Myc and anti-tubulin. (**i**) 293T cells transfected with the indicated Myc-tagged Rnd1 or empty vector in combination with VSVG-Plexin B1 were immunoprecipitated with anti-Myc, followed by immunoblotting with anti-VSVG or anti-Myc. Panels b, c, and f show one representative experiment out of two performed, whereas panels g, h, and i show one representative experiment out of three performed. Biological replicates yielded similar results. Source data is provided in Supplementary Table 8. Uncropped images of blots are shown in Supplementary Fig. 9.